Electronic Supplementary Information

How Temperature Impacts Material Properties and Photovoltaic Performance of Mixed-Halide Perovskite via Light-induced Ion Migration

Po-Kai Kung,[a] *Ming-Hsien Li,*[b] *Chen-Fu Lin,* [a] *and Peter Chen**[acd]

[a] Department of Photonics, National Cheng Kung University, Tainan, 701, Taiwan

[b] Department of Applied Materials and Optoelectronic Engineering, National Chi Nan University, Nantou, 54561, Taiwan

[c] Hierarchical Green-Energy Materials (Hi-GEM) Research Center, National Cheng Kung University, Tainan, 701, Taiwan

[d] Core Facility Center (CFC), National Cheng Kung University, Tainan, 701, Taiwan

* E-mail: petercyc@ncku.edu.tw

Experimental Section:

$CsPbIBr_2$ film fabrication: The pristine $CsPbIBr_2$ layer is synthesized by blending CsI (> 99%, Tokyo Chemical Industry) and $PbBr_2$ (99.998%, Alfa-Aesar) in 500 μL of dimethylsulfoxide (anhydrous, Sigma-Aldrich) with a molar concentration of 1M. The precursor is then spin-coated onto the FTO/TiO_2/SnO_2 substrate at 1500 rpm for 20 s followed by 5000 rpm for 60 s in a nitrogen-filled glove box. Subsequently, the coated film is annealed at 80 ℃ for 10 min and 250 ℃ for 10 min to form the perovskite film.

Device fabrication: The process initiates with fluorine-doped tin oxide (FTO) coated glass substrates, which are etched with zinc powder, initiating a reaction with hydrogen chloride to create the device pattern. The substrate undergoes cleaning through a series of steps: sonication in deionized water, acetone, and ethanol, each for 15 minutes. Following etching, a compact TiO_2 layer is spray-coated onto the FTO substrate using pyrolysis of titanium diisopropoxide bis(acetylacetonate) precursor solution diluted in ethanol (20 mM). The FTO substrate, positioned on a hot plate at 475 ℃, receives each spray delivered by an atomizer (Glaskeller) using oxygen as the carrier gas. A 10 mL diluted solution is spray-coated onto 10×20 cm^2 substrates, and the coated FTO substrate is sintered at 500 ℃ for 30 minutes. The resulting TiO_2-coated substrate is treated with ultraviolet ozone for 20 minutes, and subsequently, a tin oxide colloidal dispersion (15% in H_2O, Alfa-Aesar), diluted with deionized water solution (0.4M), is deposited using spin coating at 5000 rpm for 30 s. The as-coated tin oxide is then annealed at 150 ℃ for 30 minutes. This TiO_2/SnO_2 bilayer functions as the electron transport layer.

For the perovskite layer, the perovskite precursor is spin-coated onto the FTO/TiO_2/SnO_2 substrate at 1500 rpm for 20 s and 5000 rpm for 60 s within a nitrogen-filled glove box. The coated film is subsequently annealed at 80 ℃ for 10 minutes followed by 250 ℃ for 10 minutes to form the perovskite film. As the hole transport layer, Spiro-OMeTAD is used. The solution is prepared by dissolving 72.0 mg of spiro-OMeTAD (One Material) in 1 mL of chlorobenzene (anhydrous, 99.8%, Sigma-Aldrich). This is combined with 28.8 μL of 4-tert-butylpyridine (96%, Sigma-Aldrich) and 17.5 μL of lithium bis(trifluoromethanesulfonyl)imide (Li-TFSI) solution (520 mg of Li-TFSI salt (99.95%, Sigma-Aldrich) dissolved in 1 mL acetonitrile). The spiro-OMeTAD solution is then spin-coated onto the perovskite at 4000 rpm for 30 s within the glove box. Finally, a top electrode consisting of a 50-nm-thick layer of silver is

thermally deposited at an evaporation rate of 1 Å/s.

***Material Characterization*:** The X-ray diffraction (XRD) profile is acquired using the Bruker D8 Advance ECO XRD spectrometer, utilizing Cu Kα radiation with a scan rate of 10° min^{-1}. Photoluminescence spectra (PL) are measured employing a diode laser as the light source, operating at a wavelength of 405 nm and a power of 200 mW, through the ProtrustTech MRI measurement system. Multi-photon excited photoluminescence measurements were conducted to measure PL spectra with a laser wavelength of 930 nm, using an in-house multiphoton laser scanning microscope. The fundamental laser field was generated by a Coherent Chameleon Vision II mode-locked Ti:sapphire laser and an optical parametric oscillator, emitting at a fundamental wavelength range of 680~1600 nm with a pulse width of 140~200 fs and a repetition rate of 80 MHz. The laser was set at a wavelength of 930 nm with a frequency of 1 kHz during the measurement of PL spectra. The PL spectrum measured with a 532 nm laser is obtained using a home-built micro-photoluminescence (micro-PL) spectroscope. In this setup, a 532 nm (LSR532NL, Anjun) continuous wave laser served as the excitation source. After focusing the beam with an objective lens (Olympus MPLN5X), the PL signal was collected by a monochromator (Horiba iHR 320) equipped with a nitrogen-cooled CCD (Horiba Symphony II) and a photomultiplier (SouthPort CO.).

***Device Characterization*:** The current density-voltage (J-V) curve is obtained under AM 1.5G illumination (100 mW/cm^2) using a solar simulation system (SS-F5-3A, Enlitech) with a scan rate of 60 mV/sec. The device is connected to a source meter (Keithley 2401) to record the J-V curves. The light intensity is calibrated by certified silicon solar cells (SRC-2020-KG3, Enlitech) to verify a value of 100 mW/cm^2. The active area of the perovskite solar cell is defined as 0.15 cm^2 by a shadow mask. Impedance spectra are captured by the Autolab PGSTAT302N at a specific bias voltage, using a frequency analyzer under AM 1.5G simulated illumination. The Linkham heating stage, equipped with probes (HFS350EV-PB4), is employed to investigate the temperature-dependent behaviors of the perovskite film.

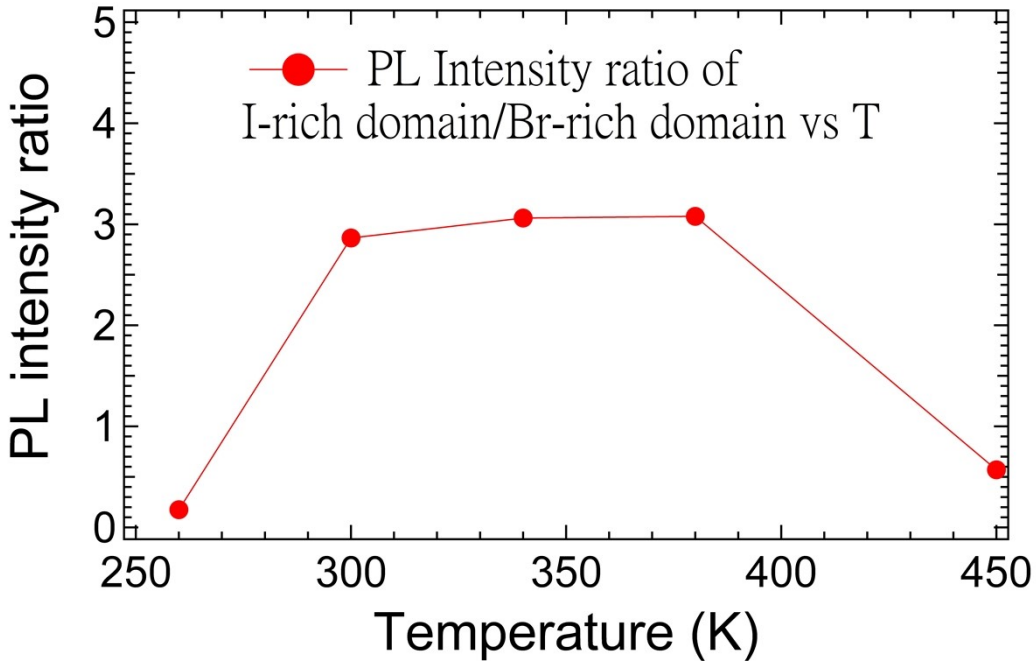

Figure S1. PL peak intensity ratio of the I-rich domain to the Br-rich domain in $CsPbIBr_2$ perovskite film at different temperatures.

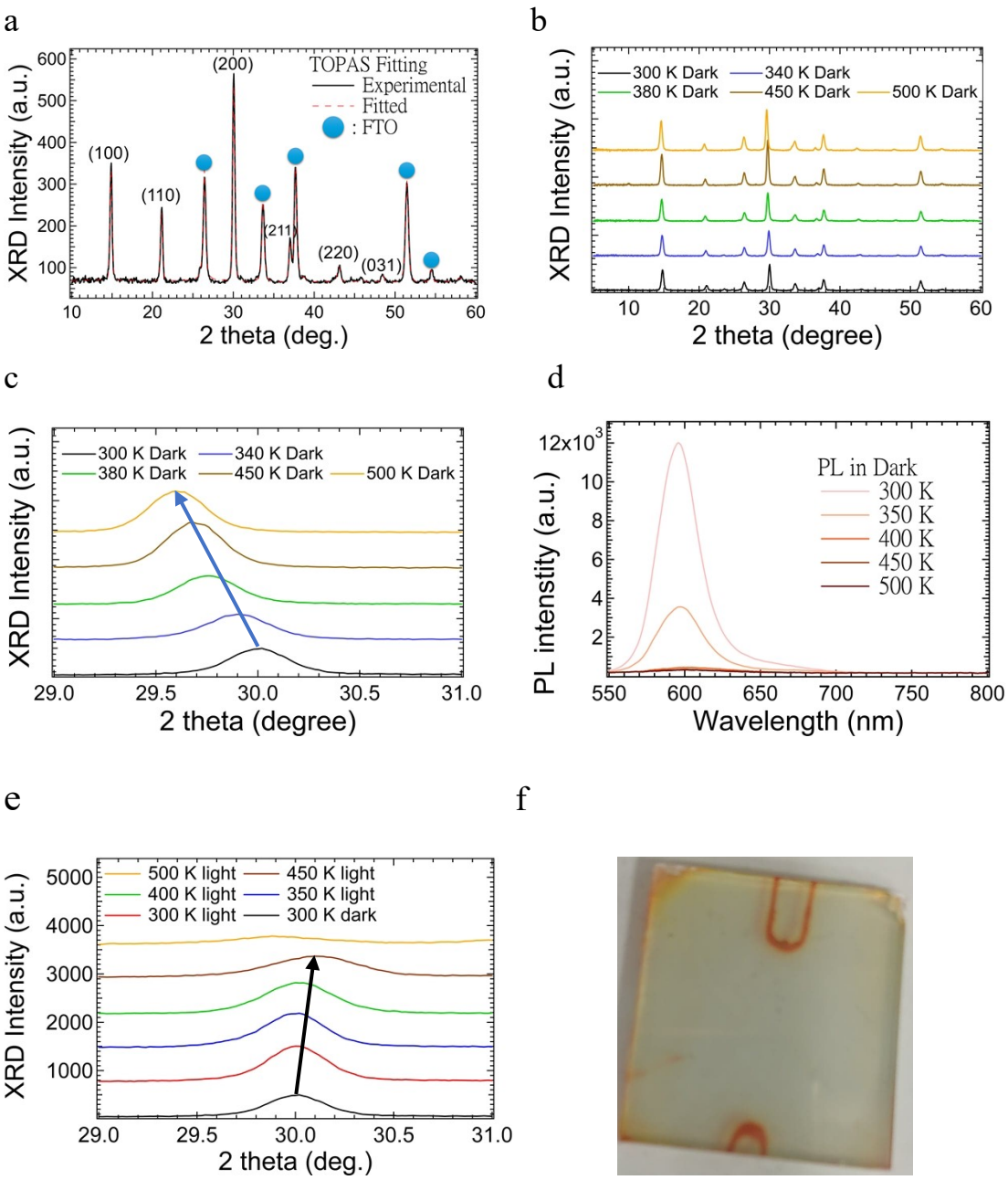

Figure S2. (a) XRD profiles of the $CsPbIBr_2$ perovskite film measured in the dark at different temperatures. (b) XRD results and a zoomed-in view (c) of the (200) plane measured at different temperatures in the dark. (d) Photoluminescence (PL) of $CsPbIBr_2$ at different temperatures measured without continuous laser illumination. (e) A zoomed-in view of XRD results measured after illumination at different temperatures. (f) Photograph of a decomposed $CsPbIBr_2$ perovskite film after being subjected to white light illumination for 10 minutes and heating at 500 K jointly.

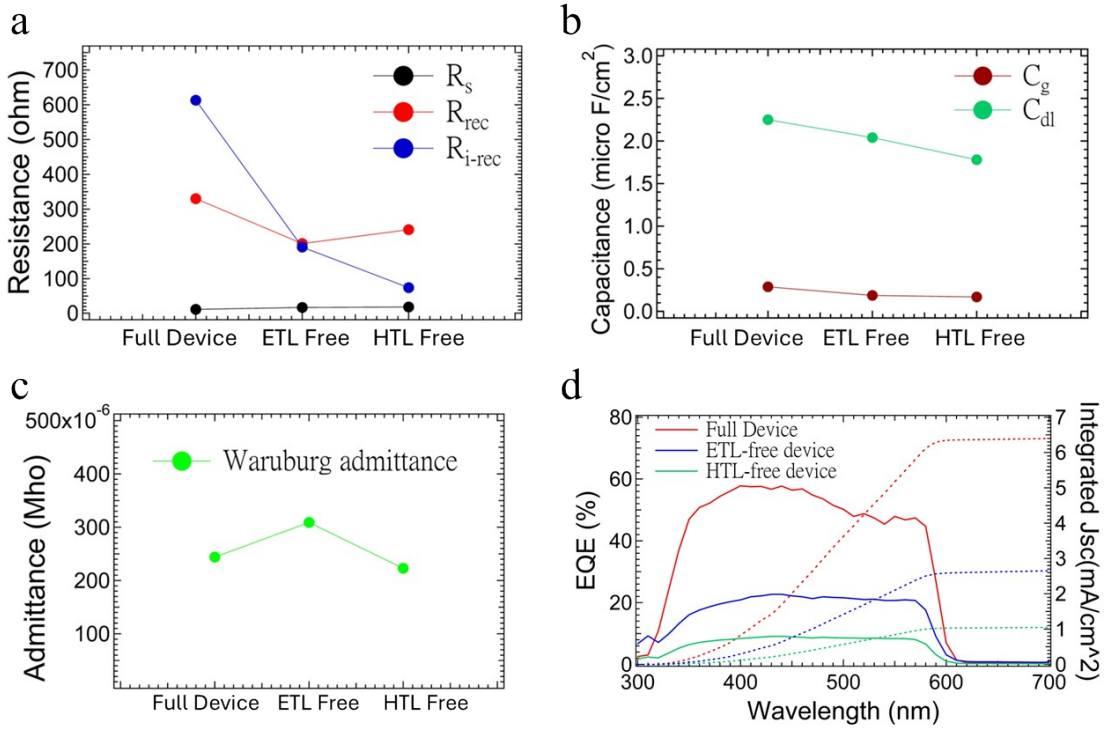

Figure S3 Various parameters extracted from the Nyquist plots of $CsPbIBr_2$ perovskite solar cells with different structures using the equivalent circuit depicted in Figure 3b. (a) R_{rec} and $R_{i\text{-}rec}$ (b) C_g and C_{dl}, and (c) Warburg admittance. (d) IPCE & integrated J_{SC} of PSCs with different device structures.

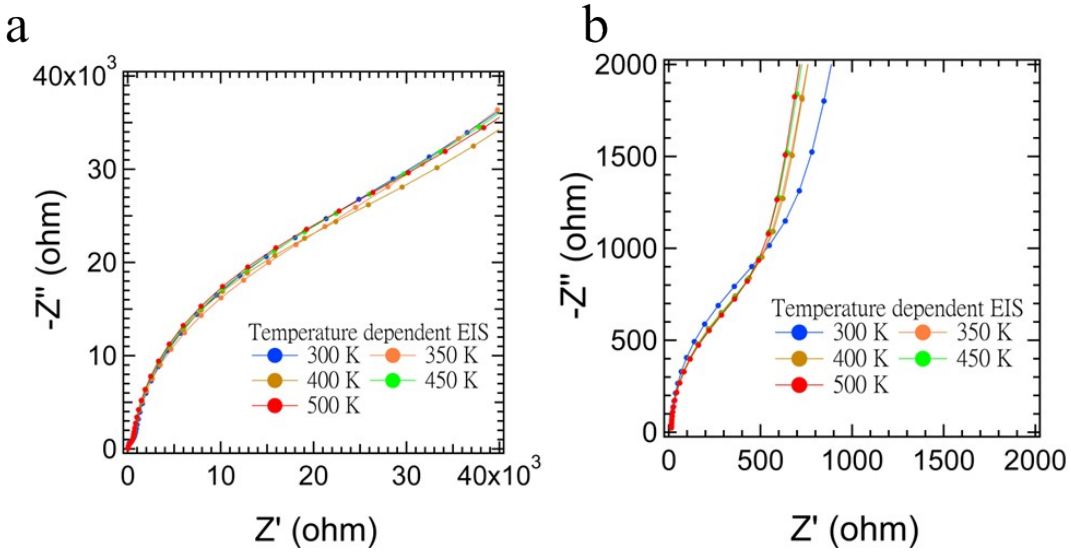

Figure S4. (a) Nyquist plots and (b) its zoon in view of $CsPbIBr_2$-based perovskite solar cells measured in the dark at different temperatures. The impedance spectra are measured under an AC perturbation with a voltage of 100 mV and frequency range from 1 to 10^6 Hz at short-circuit conditions.

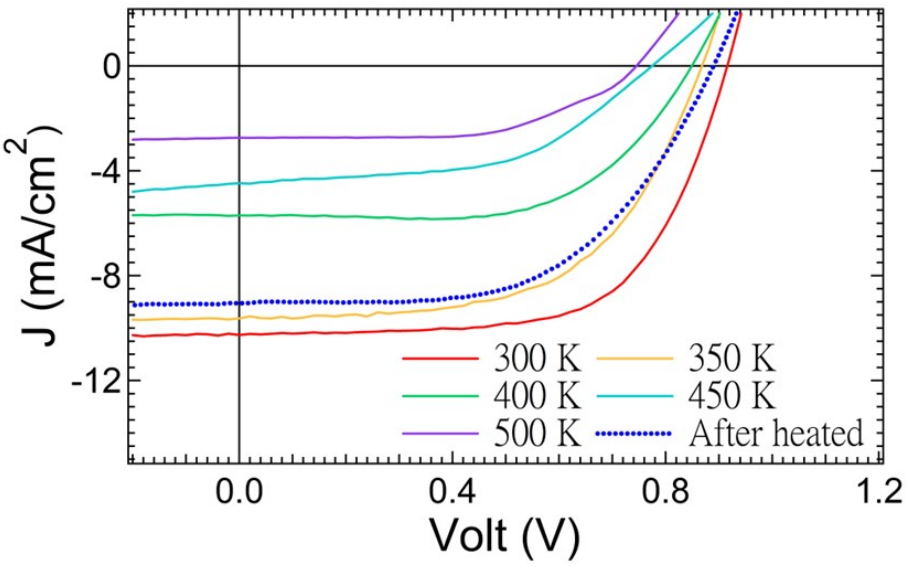

Figure S5. J-V curves measured at rising temperatures of 300 K, 350 K, 400 K, 450 K, and 500 K, as well as after cooling down. The photovoltaic performance of the perovskite solar cell before and after heating is presented in the table.

Effect of Laser Wavelength, Power, Duration, and Measuring Temperatures on Light-induced Phase Segregation:

To deconvolute the effect of laser wavelength, power, duration, and measuring temperatures, PL spectra at low temperatures varied with laser duration are first measured to present and evaluate the complete phase segregation process. As depicted in Figure S6, the photoluminescence (PL) emissions of $CsPbIBr_2$ films are measured under continuous laser illumination (λ= 405 nm, Power = 2 mW) at 200 K, 250 K, and 300 K, as shown in Figure S6a to S6c. The PL spectra at different temperatures display similar peak shift behaviors along with varying rates, as $CsPbIBr_2$ undergoes phase segregation under illumination, with the rate influenced by temperature. The differing phase segregation rates result from variations in diffusion rates, which determine the level of phase segregation over a given period. Increased temperature enhances the ionic diffusion rate, accelerating the formation of iodide-rich (I-rich) domains. Consequently, higher temperatures lead to faster phase segregation rates and enhanced PL emission intensity from I-rich domains around ~695 nm after a certain duration of laser illumination.

Here, the photoluminescence intensity ratio (PLIR) is defined as the ratio of the peak emission intensity of I-rich domains (~695 nm) to that of bromide-rich (Br-rich) domains (~595 nm) to assess the phase segregation level, as depicted in equation (1).

$$\text{PLIR} = \frac{PL\ peak\ emission\ intensity\ of\ I-rich\ domain}{PL\ peak\ emission\ intensity\ of\ Br-rich\ domain} \quad -(1)$$

An increase in PLIR value signifies greater formation of I-rich domains, indicating a higher phase segregation level. Additionally, the slope of the PLIR value over time reflects the phase segregation rate, with a steeper slope indicating a faster phase segregation process. At 300 K, the PLIR of $CsPbIBr_2$ film reaches a value of 11.33 after 60 seconds of continuous illumination, while at 250 K, it reaches 10.17 after 180 seconds, indicating slower phase segregation at lower temperatures. Furthermore, the PLIR at 200 K is even lower, with a value of 2.02 after 900 s of laser illumination, suggesting significant hindrance to phase segregation at low temperatures. This hindrance is also evidenced by the blue shift in the PL emission peak of I-rich domains at 200 K compared to that at 250 K and 300 K, indicating a stoichiometry with lower iodide content due to impeded ion migration.

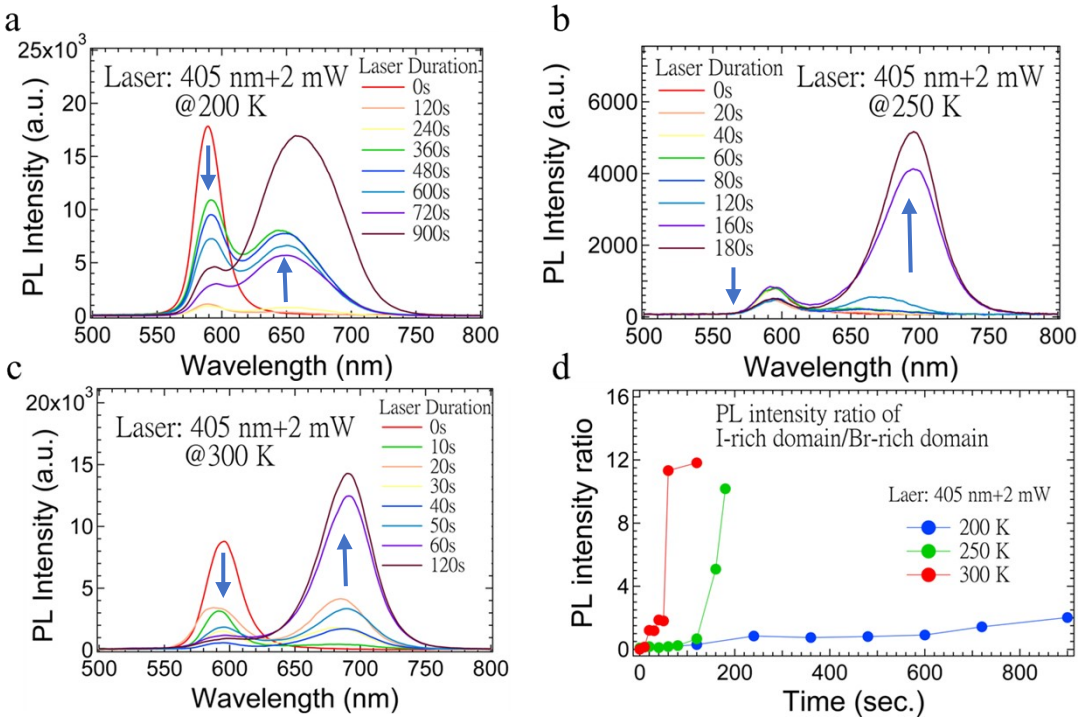

Figure S6. PL spectra of $CsPbIBr_2$ evolute with time measured at (a) 200K, (b) 250 K, and (c) 300 K. (d) PL intensity ratio (PLIR) of I-rich domain to Br-rich domain measured at different temperatures.

Regarding the effect of laser duration and wavelength on phase segregation, experiments are conducted to investigate this issue. As illustrated in Figure S7, the influence of laser duration and wavelength is examined, with these two factors jointly determining the rate and level of phase segregation processes. In Figure S7a, the PL emission of $CsPbIBr_2$ exhibits increasing emission at approximately 695 nm over time due to the occurrence of phase segregation, leading to the formation of I-rich domains with a narrower bandgap compared with $CsPbIBr_2$. Moreover, phase segregation reaches a quasi-steady state after a certain period of laser duration. Under 532 nm laser illumination with a power density of 2 mW, phase segregation reaches this quasi-steady state after 60 seconds of continuous illumination. Figure S7a demonstrates that the PL profile after 120 seconds of illumination is similar to that at 60 seconds, indicating the presence of a quasi-steady state. In short, the level of phase segregation increases with laser duration until it reaches a quasi-steady state. Such behavior is correlated with the stabilization of free energy increase induced by strain gradient resulting from polaron formation under illumination.[1]

The effect of laser wavelength on phase segregation is investigated by measuring

the PL spectra evolution over time under laser beams with different wavelengths. As shown in Figures S7a and S7b (power = 2 mW for all lasers), the PL spectra of $CsPbIBr_2$ perovskite films excited by 405 nm and 532 nm are compared. All PL spectra exhibit similar characteristics in terms of phase segregation rate and level. Regarding the phase segregation rate, the PL spectra measured at 532-nm and 405-nm excitations reach quasi-steady states after 60 seconds of continuous laser illumination, suggesting a $CsPbIBr_2$ perovskite films undergo a similar phase segregation process under exposure to 405-nm and 532-nm laser. Regarding the phase segregation level, PLIR is employed to evaluate the phase segregation level. As depicted in Figure S7c, the PLIR curves extracted from PL spectra measured with 405 nm and 532 nm lasers exhibit similar slopes and values at laser duration time = 60 seconds, indicating a similar phase segregation level and rate. Such similarity suggests that the polaron density increase induced by laser with different wavelengths is similar as the laser power, laser duration, and heating temperature are identical, leading to a similar phase segregation process.

In conclusion, the illumination duration of laser irradiation triggers phase segregation in $CsPbIBr_2$ perovskite until it reaches a quasi-steady state. Remarkably, similar levels and rates of phase segregation are observed across different laser excitation wavelengths, irrespective of the specific wavelength employed.

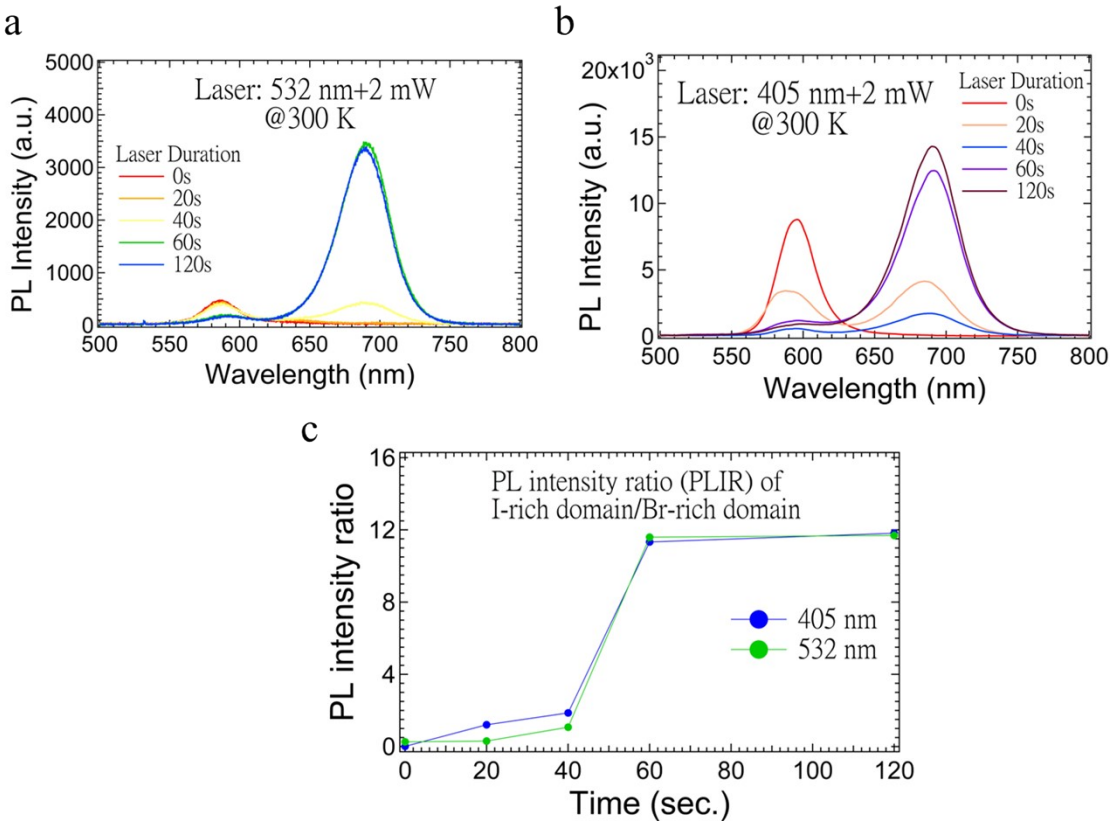

Figure S7. PL spectra of $CsPbIBr_2$ perovskite film excited by (a) 405-nm and (b) 532-nm lasers for different illumination duration. Panel (c) depicts the evolution of the PL intensity ratio (PLIR) over time. The PLIR values are extracted from the PL spectra measured with different excitation laser wavelengths.

PL spectra of $CsPbIBr_2$ are measured at different temperatures to deconvolute the effects of laser wavelengths and laser power. First, PL spectra are measured under different temperatures (300 K, 350 K, 400 K, 450 K, and 500 K) at varying durations using a laser beam with a wavelength of 405 nm and a power of 2 mW. The objective is to elucidate the evolution of the light-induced ion migration process under specific illumination conditions at different temperatures. Figures S8a to S8e demonstrate the PL spectra measured by the 405 nm laser at different temperatures. As mentioned above, the increasing temperature has two main effects on phase segregation: firstly, it enhances the phase segregation rate and level because ionic diffusion is accelerated at higher temperatures, and secondly, it facilitates the decomposition of $CsPbIBr_2$.

The PLIR is utilized to quantitatively assess both the rate and level of phase segregation. Figure S8f illustrates the PLIR extracted from PL spectra obtained at different combinations of laser durations and temperatures. The PL results from Figure

S8a to S8e are integrated in Figure S8f, depicted by curves of varying colors. PLIR allows us to observe temperature-facilitated phase segregation, evidenced by a steeper slope in the PLIR curve obtained at elevated temperatures. Additionally, the higher PLIR values demonstrated in the curves obtained at higher temperatures under specific illumination conditions and durations further indicate an increasing phase segregation level due to rising temperatures, as PLIR is proportional to the formation of I-rich domains resulting from phase segregation. For instance, the PLIR value of $CsPbIBr_2$ after 60 seconds of laser exposure increases from 11.8 at 300 K to 15.8 at 350 K, indicating temperature-facilitated phase segregation.

Conversely, the decomposition of $CsPbIBr_2$ diminishes the PLIR value due to material degradation, implying a decreased phase segregation level, as highlighted by the yellow labeling in Figure S8f. The decomposition of perovskite under simultaneous exposure to light and heat is discussed in the main article and illustrated in Figure S8e. The PL emission of the decomposition product PbI_2 is observed at a wavelength of 520 nm, indicating $CsPbIBr_2$ degradation. Consequently, as depicted in Figure S8f, a turning point is observed between laser durations of 45 seconds and 60 seconds in the PLIR curve recorded at 450 K. A low PLIR value of 1.45 following 60 seconds of laser illumination at 450 K is displayed, indicating a decrease in PLIR due to perovskite decomposition. Thus, the influence of different temperatures on phase segregation rate, phase segregation level, and material decomposition is elucidated.

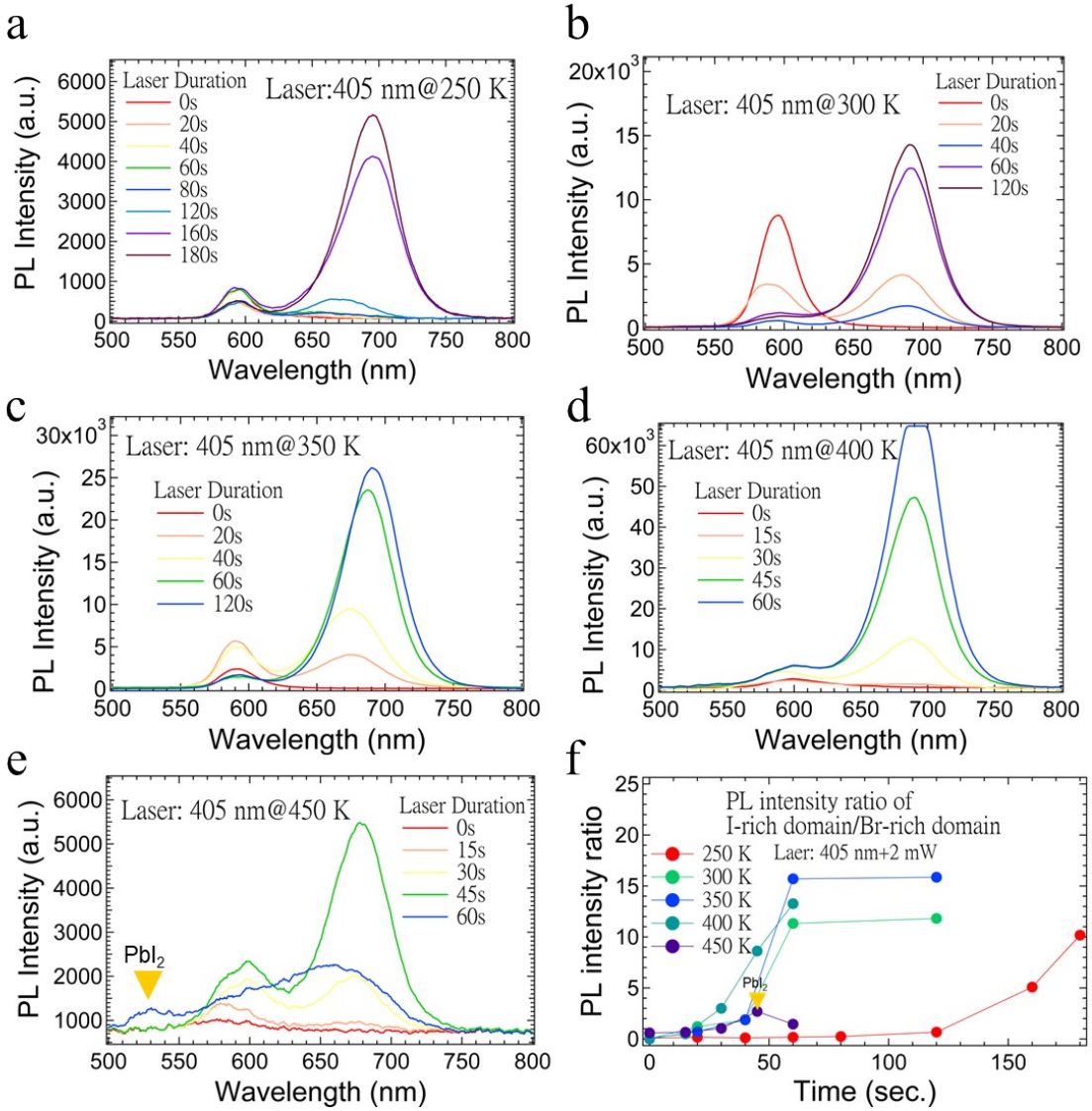

Figure S8. PL spectra obtained using a 450 nm laser (power = 2 mW) at various temperatures: (a) 250 K, (b) 300 K, (c) 350 K, (d) 400 K, and (e) 450 K. Panel (f) PLIR curves recorded at different temperatures over time.

The PLIR is further employed to investigate the influence of laser wavelengths and laser power on PL spectra measured at different temperatures. The PLIR figures shown in Figure S9 combine PL spectra measured with laser wavelengths of 405 nm and 532 nm, and different laser powers of 2 mW, 20 mW, and 100 mW at various temperatures. Several features are identified and outlined below:

(1) Higher laser power significantly accelerates phase segregation and enhances the phase segregation level at a given specific duration. For example, in Figure S9a, $CsPbIBr_2$ displays a PLIR value of 15.7 after being illuminated by a 405 nm laser with a power of 2 mW for 60 seconds at 350 K, whereas under a laser power of 20 mW, the

PLIR notably increases to 44.1 under the same laser wavelength, duration, and temperature. Such enhanced phase segregation rate is generally observed, with greater slopes shown in PLIR curves measured under higher laser power.

Additionally, higher laser power leads to a greater phase segregation level reached by the perovskite after a certain laser duration at a specific temperature. As shown in Figure S9b, the PLIR is 13.4 when the sample is illuminated by a 405 nm laser with a power of 20 mW for 40 seconds at 350 K, while under a laser power of 100 mW, the PLIR increases to 33.1 under the same laser wavelength, duration, and temperature. The increase in phase segregation level and phase segregation rate are ascribed to the increasing polaron density introduced by enhancing laser power according to our previous report.[1]

Notably, such increments in PLIR could be reduced by reversing phase segregation or decomposition of material. High laser power also leads to the reversal of phase segregation due to the elimination of strain gradient, leading to a remix of segregated halide ions, as demonstrated in our previous report and Figures S9c and S9f.[1] The PLIR curve of the sample measured with a 405/532 nm laser (power = 100 mW) at 300 K shows a turning point between laser durations of 40 seconds and 60 seconds in the PLIR curve, indicating reversed phase segregation. Nevertheless, higher laser power also introduces more pronounced decomposition in $CsPbIBr_2$. The PL spectra measured with a laser power of 2 mW (405 nm and 532 nm) show no decomposition until 450 K, while the PL spectra measured with a laser power of 100 mW demonstrate PL emission from PbI_2 at a low temperature of 350 K, indicating that rising laser power facilitates the degradation of the perovskite crystal.

(2) The laser with different wavelengths exhibits a similar phase segregation rate and phase segregation level at a certain illumination condition and temperature. As shown in Figure S9a to S9f, samples illuminated by a 405-nm or 532-nm laser with the same power at the same temperature exhibit similar PLIR values at specific laser durations, suggesting a similar phase segregation rate and level under specific conditions regardless of the laser wavelength.

(3) Increasing temperatures promote the phase segregation level, but this promotion is minor compared to that induced by power variation in our experiments. For instance, the sample illuminated with a 405 nm laser at a power of 2 mW for 60 seconds shows an increase in PLIR value from 11.33 to 15.70 as the temperature rises from 300 K to

400 K, while increasing the power from 20 mW to 100 mW increases the PLIR value from 13.4 to 33.1, as discussed in point (1). This is because the light-induced phase segregation is dominated by the polaron density induced by light and the rising temperature simply facilitates the ionic motion.

Furthermore, high temperatures result in the degradation of perovskite instead of promoting phase segregation, as no degradation is found at 300 K even when the sample is illuminated with a higher power laser of 100 mW. On the other hand, the decomposition of $CsPbIBr_2$ is widely observed at a high temperature of 450 K, regardless of the laser power and wavelength. In short, rising temperatures facilitate the phase segregation level and the decomposition of $CsPbIBr_2$ via light-induced ion migration, as discussed in the article.

(4) Combining the effects of laser power, laser wavelength, and temperatures on light-induced ion migration establishes a dynamic relation between phase segregation and material degradation, as discussed in the points above. Here, three decomposition situations are presented to complete this relation.

Firstly, perovskite degrades during phase segregation. Such degradation is observed as $CsPbIBr_2$ is illuminated with a 405 nm laser at a power of 100 mW for 60 seconds at 350 K. The degradation is evidenced by the PL spectra shown in Figure S9g, displaying PL emission from PbI_2 (520 nm), Br-rich domain (~595 nm), and I-rich domain (~695 nm) jointly.

Secondly, degradation occurs after phase segregation is complete. When $CsPbIBr_2$ is exposed to a 405 nm laser at a power of 100 mW for 60 seconds at 400 K, this degradation occurs. As shown in Figure S9h, the PL spectra exhibit joint PL emission of PbI_2 and I-rich domain, where the PL emission from the Br-rich domain is absent, indicating decomposition occurs after phase segregation.

Lastly, all perovskite material degrades into PbI_2, as shown in Figure S9i. Such degradation is observed when $CsPbIBr_2$ is subjected to a 405 nm laser at a power of 100 mW for 60 seconds at 450 K.

In conclusion, we investigate the individual and combined effects of laser wavelength, laser power, laser illumination time, and sample temperature on light-induced phase segregation. The experimental results show that as the laser illumination time increases, the segregation of perovskite material reaches a metastable state, indicating that the level of phase segregation driven by the polaron-induced strain

gradient has a limit. Laser wavelength, however, does not affect phase segregation. In contrast, an increase in laser power significantly enhances both the speed and level of phase segregation, which can be attributed to the increase in polaron density. The rising polaron density further leads to the reversal of phase segregation as introduced by high-power laser. On the other hand, temperature rise also increases the speed and level of phase segregation, although to a lesser degree compared to laser power. This is because temperature primarily promotes ion diffusion without affecting polaron density. Furthermore, higher temperatures are more likely to lead to the decomposition of perovskite material.

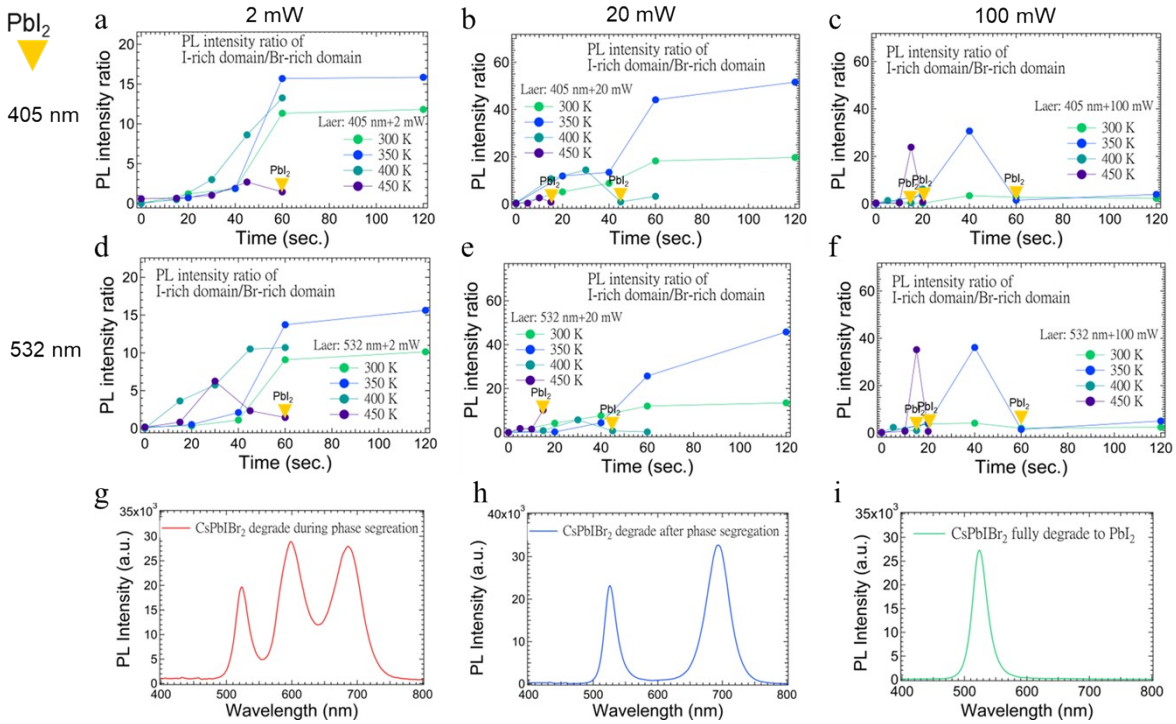

Figure S9. PLIR curves of $CsPbIBr_2$ perovskite film measured at various laser wavelengths, laser powers, illumination durations, and temperatures, depicted in panels (a)-(f). Additionally, panels (g)-(i) showcase the PL spectra corresponding to three degradation conditions of $CsPbIBr_2$ perovskite film.

Effect of Illumination Time and Heating Duration on XRD Peak Shift:

XRD experiments are conducted to explore the effects of extended duration of illumination and heating. Regarding the extended duration of illumination time, the $CsPbIBr_2$ film undergoes heating at various temperatures for 1 minute, followed by continuous white light illumination (power = 150 mW/cm², illuminated area = 2.5 x 2.5 cm²) for 10, 15, 20, and 25 minutes, respectively. The (100) plane of the $CsPbIBr_2$ crystal is monitored to observe the deformation induced by light-induced phase segregation. As depicted in Figure S10a, extended illumination time leads to an increase in XRD peak shift toward higher angles after illumination, attributed to the compressive stress introduced by facilitated phase segregation. The prolonged illumination duration promotes phase segregation, resulting in the increased formation of I-rich domains. These increasing I-rich domains introduce more compressive stress on the crystal lattice, thereby reducing the lattice constant and causing the XRD peak shift. This deformation saturates when the illumination time exceeds 20 minutes, resulting in an XRD peak shift of approximately 0.15° at 300 K.

Figure S10a also illustrates the XRD peak shift introduced by various illumination times at different measurement temperatures. The increase in measurement temperature further enhances the XRD peak shift of the (100) plane after illumination. The peak shift introduced by 25 minutes of illumination increases by 0.2° as the measurement temperature rises from 300 K to 500 K. This notable increase is also attributed to facilitated light-induced phase segregation and the formation of I-rich domains under rising temperatures. Figures S10b to S10f demonstrate the XRD results of the (100) plane before and after illumination with different illumination times at various measurement temperatures. It's worth noting that the perovskite crystal decomposes under the joint stimulation of light and heat at a high temperature of 500 K, as shown in Figure S10f, resulting in reduced XRD intensity. In summary, extended illumination and rising temperatures both increase the XRD peak shift due to the increasing formation of I-rich domains.

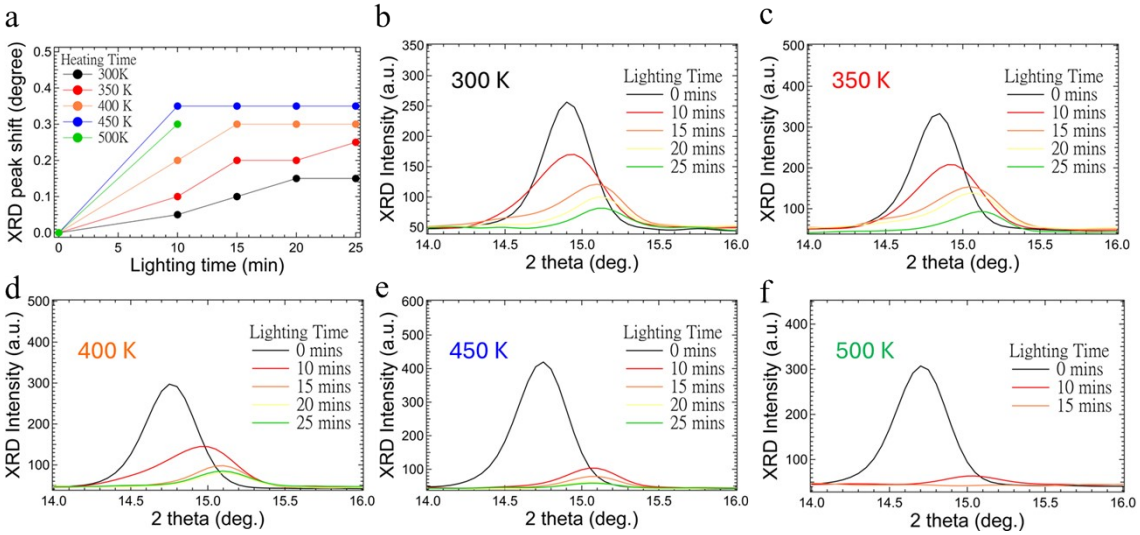

Figure S10. (a) The XRD peak shift is introduced by different illumination time measured at different temperatures. XRD results of (100) plane of $CsPbIBr_2$ crystal measured at (b) 300 K, (c) 350 K, (d) 400 K, (e) 450 K, and (f) 500 K with different illumination time.

The effect of extended heating time on XRD peak shift is examined by heating the $CsPbIBr_2$ thin film for 1, 5, 10, 15, and 20 minutes before 10 minutes of illumination on the film, respectively. As shown in Figure S11, all heating times exhibit similar peak shifts regardless of the measurement temperatures, indicating that extended heating time has a minor effect on the XRD peak shift.

Figure S11e displays the XRD peak shift of the (100) plane measured at 450 K before and after illumination. In the experiment, the sample is heated for 1 minute and followed by an illumination of 25 minutes. The temperature of 450 K introduces the maximum thermal expansion before decomposition at 500 K, and the 25 minutes of illumination induces maximum light-induced compression as shown in Figure S11. Consequently, a peak shift of 0.35° toward larger angles is observed after illumination, suggesting that the light-induced compressive stress due to light-induced phase segregation overwhelms the tensile stress induced by thermal expansion.

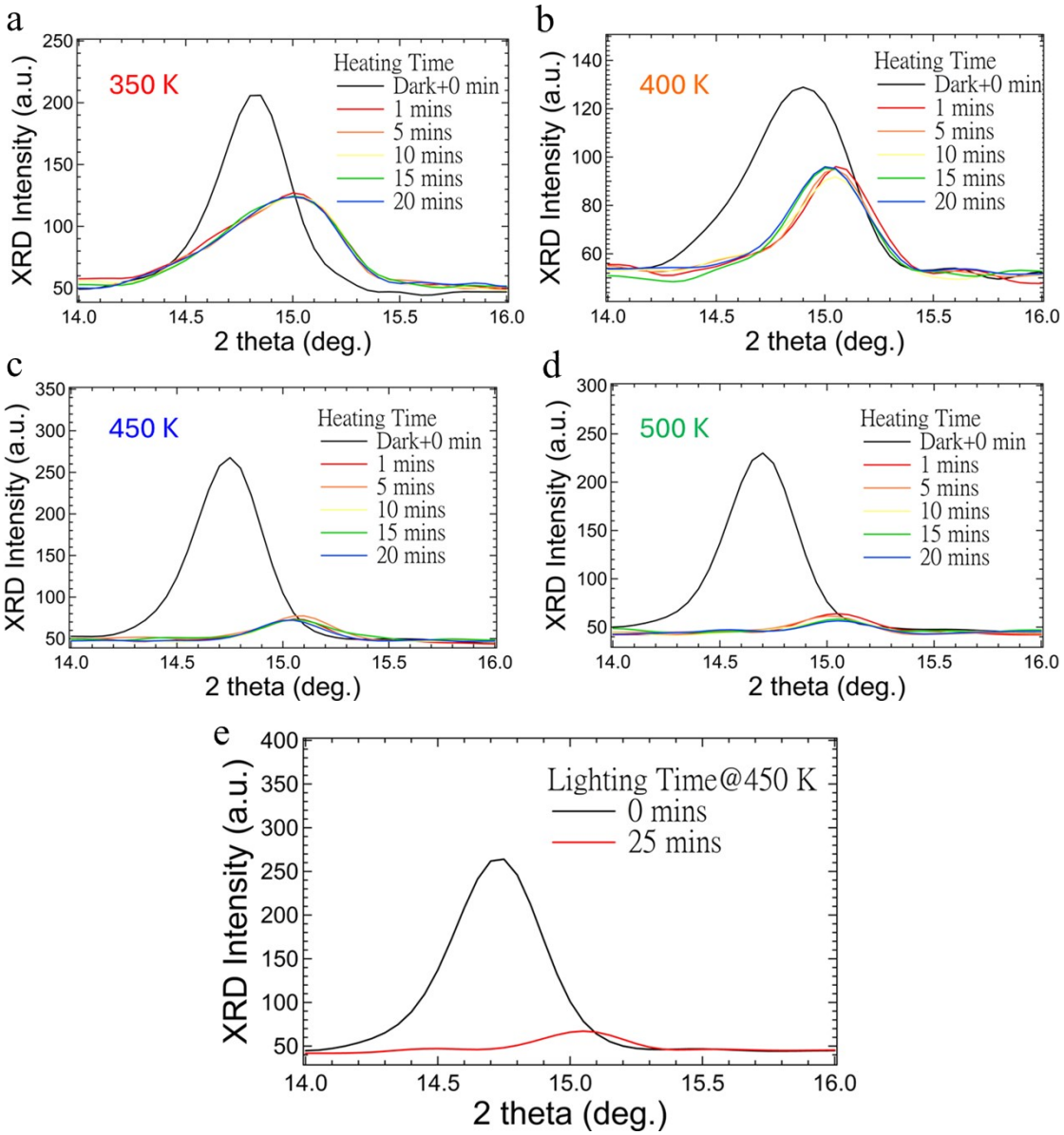

Figure S11. XRD results of (100) plane of $CsPbIBr_2$ crystal measured at (a) 350 K, (b) 400 K, (c) 450 K, and (d) 500 K with different heating time. (e) XRD result of (100) plane measured after 1 minute of heating and 25 minutes of illumination.

Table S1. Series (R_s), recombination (R_{rec}), and charge transfer resistances (R_{ct}), geometric (C_g) and double-layer capacitances (C_{dl}) extracted from Nyquist plots of $CsPbIBr_2$ perovskite solar cells with different structures (full device, w/o TiO_2+SnO_2 (ETL-free device), and w/o Spiro (HTL-free device)).

	Full cell	ETL free Device	HTL free Device
C_g (F/cm^2)	2.70E-07	1.87E-07	1.69E-07
C_{dl} (F/cm^2)	3.76E-06	2.04E-06	1.78E-06
W (Mho)	1.63E-04	3.09E-04	2.23E-04
R_s (Ω)	1.23E+01	1.73E+01	2.47E+01
R_{rec} (Ω)	3.48E+02	2.01E+02	2.41E+02
$R_{i\text{-}rec}$ (Ω)	6.26E+02	1.91E+02	7.43E+01

Table S2. Fitted parameters extracted from Nyquist plots of $CsPbIBr_2$ perovskite solar cells measured at different temperatures.

	300 K	350 K	400 K	450 K	500 K
C_g (F/cm^2)	2.88E-07	2.70E-07	2.60E-07	2.59E-07	1.84E-07
C_{dl} (F/cm^2)	4.34E-06	2.25E-06	1.23E-06	7.73E-07	7.07E-07
W (Mho)	1.26E-04	1.43E-04	1.45E-04	1.54E-04	2.44E-04
R_s (Ω)	1.19E+01	1.21E+01	1.70E+01	1.36E+01	1.88E+01
R_{rec} (Ω)	3.30E+02	3.09E+02	2.89E+02	2.55E+02	1.78E+02
$R_{i\text{-}rec}$ (Ω)	6.13E+02	6.15E+02	5.12E+02	4.48E+02	4.00E+02

Table S3. The mean values and standard deviations of power conversion efficiency of $CsPbIBr_2$ solar cell measured at different temperatures.

Temperautre (K)	No. of Devices	PCE (%)
300	20	5.06 ± 0.303
350	20	4.45 ± 0.336
400	20	4.14 ± 0.364
450	20	3.22 ± 0.467
500	20	1.12 ± 0.465

Table S4. PV parameters of $CsPbIBr_2$-based perovskite solar cells measured before/after heated.

	PCE (%)	V_{OC} (V)	J_{SC} (mA/cm^2)	FF (%)
Before heated	5.92	0.91	10.23	64.2
After heated	4.54	0.89	9.04	56.4

Table S5. Photovoltaic performance of representative perovskite solar cells for stability test.

Temperautre (K)	Original PCE (%)	Original V_{OC} (V)	Original J_{SC} (mA/cm^2)	Original FF (%)
300	5.24	1.1	8.58	55.9
350	4.54	0.89	9.04	56.5
400	3.76	0.85	8.17	54
450	3.04	0.82	6.3	59.11
500	1.69	0.74	5.4	42.5

Table S6. Mean value and standard deviation of normalized PCE (%) evolutes with time at different temperatures.

Normalezd PCE (%) evolutes with time at different heating temperatures							
	300 K	350 K	400 K		450 K		500 K
0 hr	100.00	100.00	100	0 hr	100	0 hr	100
1 hr	97.37 ± 2.15	97.90 ± 0.75	80.84 ± 4.08	0.33 hr	75.13 ± 4.59	0.25 hr	66.94 ± 9.79
2 hr	95.40 ± 2.13	74.70 ± 4	66.72 ± 5.06	0.67 hr	56.12 ± 5.41	0.33 hr	59.03 ± 5.25
3 hr	94.13 ± 1.97	66.7 ± 7.62	37.75 ± 4.2	1 hr	27.31 ± 3.15	0.5 hr	1.97 ± 2.78
4 hr	92.25 ± 2.64	60.61 ±7.74	0.53 ± 0.49	1.33 hr	24.31 ± 1.67		
5 hr	90.7 ± 4.27	49.27 ± 6.88		1.67 hr	7.432 ± 2.23		
6 hr	88.31 ± 3.13	29.59 ± 4.21		2 hr	1.53 ± 1.18		
7 hr	85.87 ± 3.4	6.03 ± 3.43					
8 hr	79.30 ± 1.32						

Reference

1. P.-K. Kung, K.-I. Lin, C.-S. Wu, M.-H. Li, C.-R. Chan, R. Rajendran, C.-F. Lin and P. Chen, *The Journal of Physical Chemistry Letters*, 2022, **13**, 6944-6955.